Solid–liquid coexistence of neon, argon, krypton, and xenon studied by simulations

View Online   Export Citation   CrossMark

Aditya N. Singh,[1] (iD) Jeppe C. Dyre,[2] (iD) and Ulf R. Pedersen[2,a)] (iD)

AFFILIATIONS

[1] Department of Chemistry, University of California, Berkeley, California 94720, USA and Theoretical Chemistry Institute
and Department of Chemistry, University of Wisconsin-Madison, 1101 University Avenue, Madison, Wisconsin 53703, USA
[2] Glass and Time, IMFUFA, Department of Science and Environment, Roskilde University, P. O. Box 260,
DK-4000 Roskilde, Denmark

[a)] Author to whom correspondence should be addressed: ulf@urp.dk

ABSTRACT

The noble elements constitute the simplest group of atoms. At low temperatures or high pressures, they freeze into the face-centered cubic (fcc) crystal structure (except helium). This paper investigates neon, argon, krypton, and xenon by molecular dynamics using the simplified atomic potentials recently proposed by Deiters and Sadus [J. Chem. Phys. **150**, 134504 (2019)], which are parameterized using data from accurate *ab initio* quantum-mechanical calculations by the coupled-cluster approach at the single-double-triple level. We compute the fcc freezing lines and find good agreement with the empirical values. At low pressures, predictions are improved by including many-body corrections. Hidden scale invariance of the potential-energy function is established by showing that mean-squared displacement and the static structure factor are invariant along the lines of constant excess entropy (isomorphs). The isomorph theory of melting [Pedersen *et al.*, Nat. Commun. **7**, 12386 (2016)] is used to predict from simulations at a single state point the freezing line's shape, the entropy of melting, and the Lindemann parameter of the crystal at melting. Finally, our results suggest that the body-centered cubic crystal is the thermodynamically stable phase at high pressures.

I. INTRODUCTION

The thermodynamic and transport properties of condensed matter systems are determined by their potential-energy functions.[1] For a class of systems, the potential-energy function exhibits "hidden scale invariance,"[2] making the phase diagram effectively one dimensional; thus, density and temperature collapse into a single parameter.[2–13] This scaling, referred to as density scaling, has been demonstrated for simple model potentials,[7,8,14–16] atomic liquids,[17–22] and molecular liquids.[4–6,9,23] In this paper, we investigate the noble elements neon (Ne), argon (Ar), krypton (Kr), and xenon (Xe) using a potential proposed recently from accurate *ab initio* calculations.[24] We find that the energy surface obeys hidden scale invariance in the investigated part of the phase diagram and show how this fact can be used to predict the shape of the melting lines.[25]

Specifically, we investigate below the simplified *ab initio* atomic potential (SAAP) recently suggested by Deiters and Sadus.[24] This potential is parameterized for the noble elements Ne, Ar, Kr, and Xe from quantum-mechanical calculations using the coupled-cluster approach[26,27] on the coupled-cluster single-double-triple [CCSD(T)] theoretical level.[28] This approach is considered the gold standard of quantum chemistry[29] and has been shown to give accurate prediction for the noble elements.[27,30–33]

We consider monatomic systems of N particles of mass m confined to the volume V with periodic boundaries with number density $\rho = N/V$. Let $\mathbf{R} \equiv (\mathbf{r}_1, \mathbf{r}_2, \mathbf{r}_3, \ldots, \mathbf{r}_N)$ be the collective coordinate vector. The potential-energy function is the sum of pair-potential contributions,

$$U(\mathbf{R}) = \sum_{i>j}^{N} v(|\mathbf{r}_i - \mathbf{r}_j|), \qquad (1)$$

in which the dimensionless SAAP pair potential $\phi(x) \equiv v(x\sigma)/\varepsilon$ is given by

$$\phi(x) = \frac{a_0 \exp(a_1 x)/x + a_2 \exp(a_3 x) + a_4}{1 + a_5 x^6}. \qquad (2)$$

The six a parameters[24] are determined by fitting to the results of the above-mentioned *ab initio* calculations on dimers.[26] In the simulations reported below, the pair potential is truncated and shifted at $r_c = 4\sigma$. The truncation leads to tail corrections of the full potential.[34] Pressure corrections are estimated to range from $-0.3\varepsilon/\sigma^3$ to $-0.1\varepsilon/\sigma^3$ depending on the state points (see the supplementary material).

An advantage of the SAAP is that it is computationally efficient and, at the same time, accurately represents the underlying *ab initio* calculations.[24] Figure 1(a) shows the SAAP of Ar (in MD units defined by $\varepsilon = \sigma = 1$). The SAAP is compared to the Lennard-Jones (LJ) pair potential $4[x^{-12} - x^{-6}]$ (green dashed line; simulation details for the LJ system can be found in Ref. 25). As noted by Thiel and Alder,[35] the LJ potential is very steep at short distances [Fig. 1(b)] but overall describes well the SAAP, though being a bit broader. In comparison, the exponential repulsive (EXP) pair potential $4 \cdot 10^5 \exp(-12x)$[11,12,16,36,37] (red dashed lines) approximates well the SAAP at short distances. This is consistent with the interpretation of high-pressure compression experiments, the so-called shock Hugoniots.[35,38]

Simulations were conducted using the RUMD software package v3.4[39] (the SAAP was implemented in v3.4 by hand but is now included in v3.5). We studied systems of $N = 5120$ particles in an elongated orthorhombic simulation cell. The box lengths in the y and z directions are identical, while the box length in the x direction is 2.5 times longer to accommodate the below described *interface-pinning* simulations. More details of simulation algorithms are given in the supplementary material.

In order to illustrate the theory, this paper starts by treating in detail the case of argon (Secs. II–IV). Sections V–VII report the analogous results for neon, krypton, and xenon. Section VIII gives a brief summary.
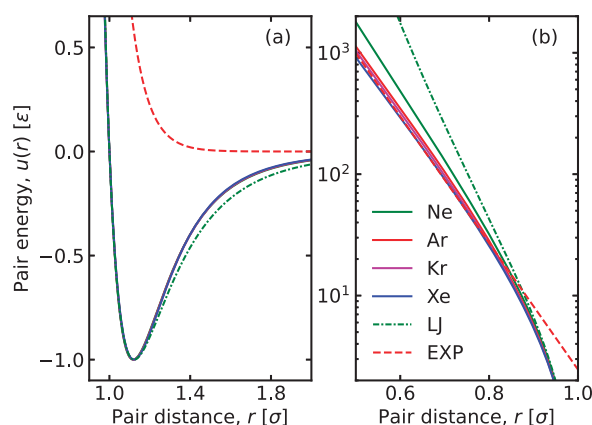

FIG. 1. (a) The solid lines show the SAAP pair potential for Ne (green), Ar (red), Kr (magenta), and Xe (blue). For comparison, the dashed lines show the LJ (green) and the EXP (red) pair potentials. (b) The pair potentials at short distances on a logarithmic scale.

II. THE COEXISTENCE LINE OF ARGON

The Ar coexistence line between the liquid and the fcc solid phases is determined as follows (the supplementary material includes details of the pair potential and the simulation algorithm): First, we use the interface-pinning method[41–49] to compute the solid–liquid chemical potential difference $\Delta\mu$ at temperature $T_0 = 2\varepsilon/k_B$ (287 K) for a range of fcc lattice constants corresponding to different pressures. $\Delta\mu$ is computed from the thermodynamic force on a solid–liquid interface in an equilibrium simulation with an auxiliary potential that biases the system toward two-phase configurations. To account for slow fluctuations of the solid–liquid interface, two-phase simulations were eight times longer than the bulk simulations. We find that the coexistence pressure ($\Delta\mu = 0$) is $p_0 = 22.591(4)\varepsilon/\sigma^3$ at T_0 in which the number in parentheses indicates the estimated statistical uncertainty on the least significant digit. Other coexistence points are then determined by numerical integration along temperatures on the coexistence line using the fourth-order Runge–Kutta (RK4) algorithm.[50] The required slopes dp/dT are computed from isobaric simulations of a solid and a liquid using the Clausius–Clapeyron relation:[51] if $\Delta V_m = V_{\text{liquid}} - V_{\text{solid}}$ is the volume difference between liquid and solid and $\Delta S_m = (U_{\text{liquid}} - U_{\text{solid}} + p\Delta V_m)/T$ is the entropy difference, the local slope is computed from[51]

$$\frac{dp}{dT} = \frac{\Delta S_m}{\Delta V_m}. \qquad (3)$$

The RK4 algorithm requires four slope evaluations; thus, each integration step involves four simulations of a liquid and four simulations of a solid. This recipe for computing solid–liquid coexistence lines was suggested in Ref. 37. As a consistency check, we have confirmed that the gradient of the central difference of the computed melting line agrees with $\Delta S_m/\Delta V_m$ [Eq. (3)]. This technique is in the class of *Gibbs–Duhem integration* methods suggested by Kofke.[51] Details are provided in the supplementary material.

The coexistence line for Ar is shown as a black solid line in Fig. 2(a) together with the empirical (experimental) values[40] shown with a red dashed line. The agreement is good; however, as seen in the inset, the SAAP slightly overestimates the coexistence temperature at a given pressure. This may be due to the missing many-body interactions of the SAAP. To investigate this, following the suggestion by Deiters and Sadus,[52] we apply a mean-field correction that only depends on the average density of a bulk phase. For the correction of the coexistence pressure, we take the different densities of the phases into account. Let $\bar{\rho} = 2/(v_s + v_l)$ be the average density between the two phases (where v_s is the solid phase volume per particle) at a given coexistence point ($T^{\text{SAAP}}, p^{\text{SAAP}}$) computed with the SAAP. The corrected state point is then

$$(T_{\text{corr}}, p_{\text{corr}}) = (\varepsilon_{\text{corr}} T^{\text{SAAP}}, \varepsilon_{\text{corr}} p^{\text{SAAP}}), \qquad (4)$$

in which

$$\varepsilon_{\text{corr}} = 1 - \frac{\lambda \nu \bar{\rho}}{\varepsilon \sigma^6} \qquad (5)$$

is an energetic correction parameter of the ε in Eq. (1), $\nu/\varepsilon\sigma^9 = 0.068\,753\,6$ is the Axilrod–Teller–Muto parameter[53] of Ref. 52, and λ is a parameter obtained from analyzing two-body and three-body simulation data.[54] For simplicity, we set λ to unity. The blue
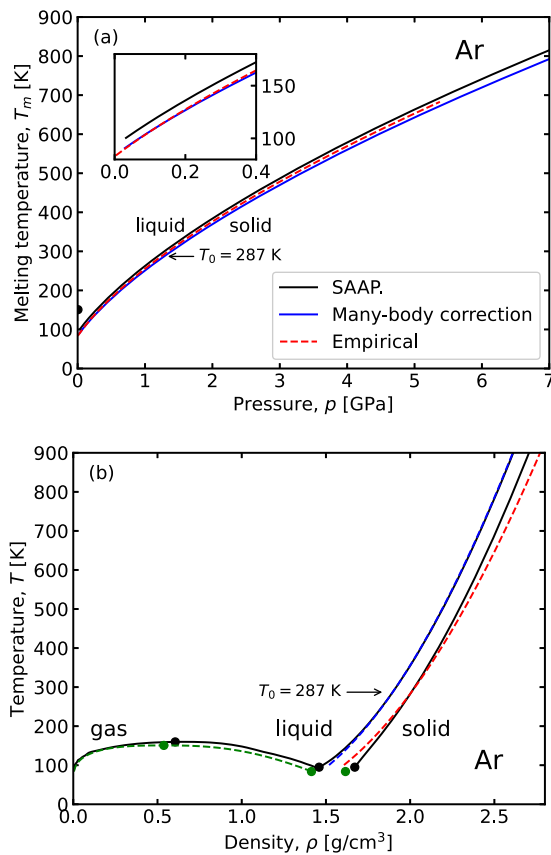
FIG. 2. (a) The solid–liquid coexistence line of Ar in the pT-plane. The black solid line is the melting temperature computed for the SAAP by first using the interface-pinning method at $T_0 = 287$ K and then using a fourth-order Runge–Kutta integration of the Clausius–Clapeyron identity to determine remaining coexistence points. The blue solid line is a mean-field correction taking into account the missing many-body interactions of the SAAP (see the main text), and the red dashed line is the empirical (experimental) melting line of Datchi *et al.*[40] The black dot on the y-axis is the gas–liquid critical point. The inset is a zoom-in on low pressures. (b) The Ar phase diagram in the ρT-plane. The black solid lines are the boundaries of the phases. The three black dots are the critical point and the triple points of the liquid and solid phases, respectively. The green dots and dashed lines are empirical values. The blue and red dashed lines are a liquid and a solid isomorph based on the SAAP, (see Sec. III). The statistical errors are small in comparison to the thickness of the lines.

solid line on Fig. 2 shows the corrected melting line. The correction is small, but it explains the deviations from the experimental melting line at low pressures [inset of Fig. 2(a)]. At high pressures, however, the uncorrected melting line is better than the corrected one. This suggests that many-body interactions are not important at high pressures, or that the above correction is inaccurate. For the remainder of the paper, we ignore many-body corrections, but note that inclusion of many-body effects will give some minor quantitative changes to our result. We also note that tail corrections to the truncated potentials will play a role (see the supplementary material). A study of these effects is left to future studies.

III. HIDDEN SCALE INVARIANCE OF ARGON

The following gives a brief introduction to the theory of systems with hidden scale invariance, known as isomorph theory,[2,7,8,10,12] and applies it to the Ar parametrization of the SAAP.

Consider two same-density configurations $\mathbf{R}_a$ and $\mathbf{R}_b$ where

$$U(\mathbf{R}_a) < U(\mathbf{R}_b). \tag{6}$$

If the energy surface is scale invariant, it follows that

$$U(\lambda\mathbf{R}_a) < U(\lambda\mathbf{R}_b), \tag{7}$$

where λ determines the magnitude of an affine scaling of all particle positions (and thus also the change of density). Scale invariance is trivial if U is a sum of inverse power-laws with the same exponent, so-called conformal potentials.[4,5,7,14,15,55] However, the SAAP, LJ, and EXP potentials are not conformal. Nevertheless, depending on the state point in question, the above scaling can be a good approximation for relevant configurations. In that case, we refer to the scaling as *hidden* because it reflects an approximate property that is not obvious from the mathematical expression for the potential-energy function. From the definition of hidden scale invariance, it may be shown that there are lines in the thermodynamic phase diagram, referred to as isomorphs, along which structure, dynamics, and certain thermodynamics quantities are invariant in "reduced" units.[2,8] These units are state-point dependent and defined from a combination of particle mass m, the number density ρ, and the thermal energy $k_B T$.[2,8] Isomorphs are defined as lines where the excess entropy S_{ex} is constant, i.e., an isomorph is a configurational adiabat. Here, "ex" refers to the entropy *in excess* of the ideal gas entropy at the same density and temperature,[1,3,22,56]

$$S_{ex}(\rho, T) = S(\rho, T) - S_{id}(\rho, T). \tag{8}$$

We note that the above equation in chemical thermodynamics is referred to as the *residual* entropy[57,58] and should not be confused with the *excess entropy* defined in relation to ideal mixtures.[3,59,60]

Scaling by reference to the excess entropy was first suggested by Rosenfeld[3] and has recently gained renewed interest.[13,20,56,57,61,62] As mentioned, a configurational adiabat is referred to as an *isomorph* for state points with hidden scale invariance, which implies invariant reduced structure and dynamics (*isomorph* is the greek word for same-shape). The slope of a configurational adiabat (and thus an isomorph) in the double logarithmic temperature-density plane,

$$\gamma \equiv \left.\frac{\partial \ln T}{\partial \ln \rho}\right|_{S_{ex}}, \tag{9}$$

can be computed from the fluctuations of virial W and potential energy U in the NVT (canonical) ensemble as[8]

$$\gamma = \frac{\langle \Delta W \Delta U \rangle}{\langle (\Delta U)^2 \rangle}. \tag{10}$$

Here, $\langle \cdots \rangle$ is the expectation value and Δ denotes the deviation from the mean (in practice, $\langle \cdots \rangle$'s are computed as time-averages). The dashed lines in Fig. 2(b) show a liquid and a solid isomorph

TABLE I. Thermodynamic data for SAAP estimated coexistence state points at the reference temperature $T_0 = 2\varepsilon/k_B$ obtained by the interface-pinning method.[41,42]

	ε/k_B (K)	σ (Å)	p_0 (ε/σ^3)	V_l/N (σ^3)	V_s/N (σ^3)	$\Delta V_m/N$ (σ^3)	$\Delta S_m/N$ (k_B)
Ne	42.36	2.759	21.911(2)	0.934 82(2)	0.880 69(2)	0.054 128(8)	1.097 07(13)
Ar	143.5	3.355	22.591(4)	0.926 12(3)	0.874 89(3)	0.051 227(11)	1.085 15(13)
Kr	201.1	3.580	23.079(2)	0.919 99(2)	0.870 75(2)	0.049 2320(9)	1.073 43(16)
Xe	280.2	3.901	23.423(4)	0.916 23(3)	0.868 28(3)	0.047 951(7)	1.067 53(11)
LJ			20.8270(8)	0.940 160(8)	0.882 777(7)	0.057 388(7)	1.097 27(13)

computed by numerical integration of Eq. (9) using the RK4 method from the reference state point (T_0, ρ_0) given in Table I.

Figure 3(a) shows that the liquid structure is indeed invariant along the isomorph. This is done by investigating the static structure factor

$$S(\mathbf{q}) = \langle |\rho_\mathbf{q}|^2 \rangle, \quad (11)$$

where

$$\rho_\mathbf{q} = \sum_{n=1}^{N} \exp(i\mathbf{q} \cdot \mathbf{r}_n)/\sqrt{N}. \quad (12)$$

For a liquid, the structure factor depends only on the wave-vector length denoted by q. Figure 3(b) shows $S(q)$ for state points along an isochore starting near the triple point. Figures 3(c) and 3(d) show $S(q)$ for the fcc solid along state points of an isomorph and an isotherm, respectively. As for the liquid, the structure of the solid is isomorph invariant to a good approximation. We note that the long-wavelength (small q) limit of the structure factor does not scale well [inset of Fig. 3(a)]. This limit is proportional to the isothermal compressibility, which is not isomorph invariant even in reduced units.[18]

Figure 4(a) shows that the dynamics is invariant along the liquid isomorph. This is done by investigating the mean-squared displacement and the diffusion coefficient (inset) computed from its long-time limit (dashed line). Figure 4(b) shows the same along an isochore.

The microscopic virial function is defined by

$$W(\mathbf{R}) = -\sum_{i>j} |\mathbf{r}_i - \mathbf{r}_j| v'(|\mathbf{r}_i - \mathbf{r}_j|)/3, \quad (13)$$

where v' is the first derivative of the pair potential. The virial is referred to as the "potential part of the pressure" since the pressure p is given by the relation

$$pV = Nk_BT + W, \quad (14)$$

where $W = \langle W(\mathbf{R}) \rangle$. Systems with hidden scale invariance are sometimes referred to as "strongly correlating"[7] because the fluctuations of virial and potential energy are strongly correlated in the NVT (canonical) ensemble. Figure 5 shows the Pearson correlation coefficient R between $W(\mathbf{R})$ and $U(\mathbf{R})$ of the canonical ensemble,

$$R = \frac{\langle \Delta W \Delta U \rangle}{\sqrt{\langle (\Delta W)^2 \rangle \langle (\Delta U)^2 \rangle}}, \quad (15)$$

for the liquid (blue points) and the crystal isomorph (red points). The correlation is strong as expected from the invariant structure and dynamics (Figs. 3 and 4), and we find $R > 0.94$ for all investigated
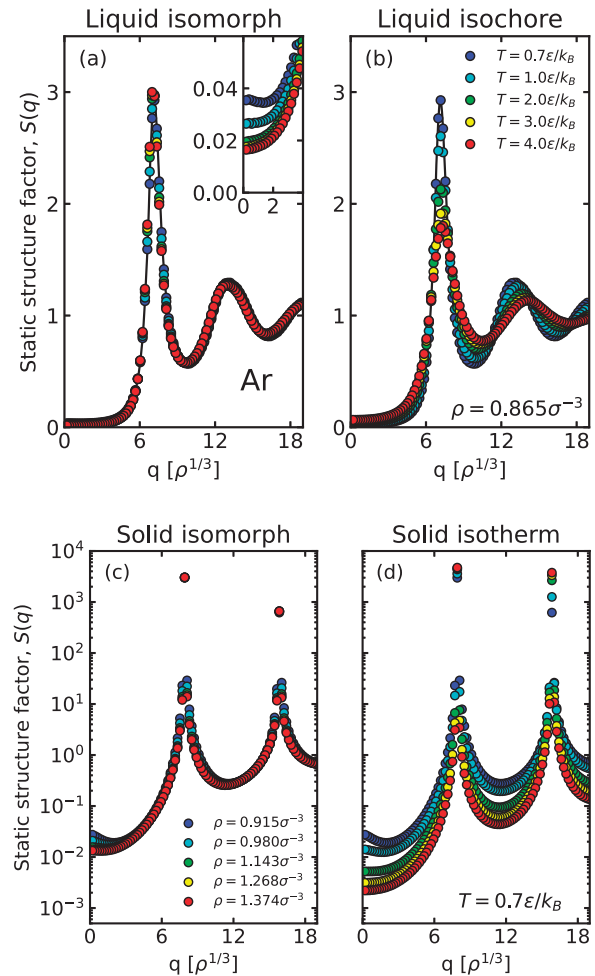

FIG. 3. (a) The static structure factor, $S(q)$, along the liquid isomorph of SAAP with Ar parameters near the freezing line [blue dashed line in Fig. 2(b)]. The first axis gives q in units of $\rho^{1/3}$. The structure is invariant along the isomorph. The solid line is a guide to the eye. The inset zooms in on $S(q)$ for small q vectors, demonstrating that the isothermal compressibility is not isomorph invariant because $S(0)$ is not. (b) $S(q)$ along the liquid isochore with the same density as the state point on the isomorph with temperature $T = 0.7\varepsilon/k_B$. (c) $S(q)$ with the wave-vector $\mathbf{q}$ perpendicular to the (100) lattice plane of the fcc solid along isomorphic state points [red dashed line in Fig. 2(b)]. The first two Bragg peaks are shown. (d) $S(q)$ of the fcc solid along the $T = 0.7\varepsilon/k_B$ isotherm for the same range of densities as the isomorph. The statistical errors are small in comparison to the symbols for all the shown data.
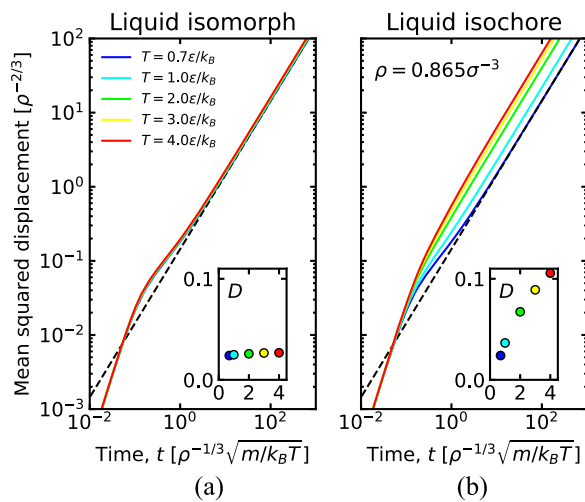
FIG. 4. (a) Reduced-unit mean-squared displacement along the liquid SAAP isomorph of Ar near the freezing line [blue dashed line in Fig. 2(b)]. The collapse of the data demonstrates that the dynamics is invariant along the isomorph. The inset demonstrates isomorph invariance of the diffusion coefficient D in reduced plotted as a function of the temperature. The reduced diffusion coefficient is computed from the long-time limit of the reduced mean-squared displacement. (b) Reduced mean-squared displacement along the liquid isochore with the same density as the state point on the isomorph with temperature $T = 0.7\varepsilon/k_B$. The statistical errors are small in comparison to the thickness of the lines or symbols for all the shown data.

state points. The correlation increases with increasing temperature (and density). This is consistent with the fact that the structure is more invariant on the high-temperature part of the configurational adiabat (inset of Fig. 5).
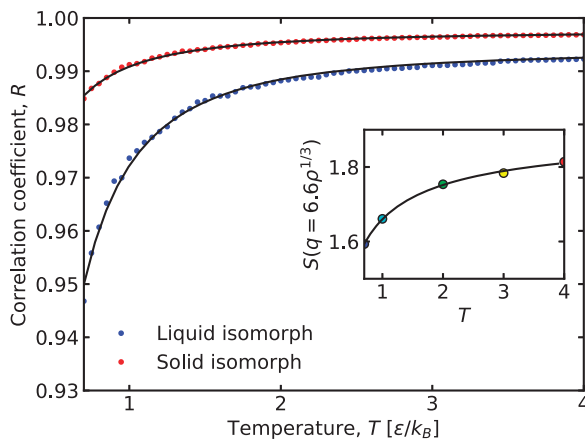

FIG. 5. The Pearson correlation coefficient R between virial W and potential energy U [Eq. (15)] along the liquid isomorph (blue points) and the solid isomorph (red points) of SAAP with Ar parameters [Fig. 2(a)]. The solid lines are guides to the eye. The correlation coefficient approaches unity with increasing temperature. The inset shows the static structure factor $S(q = 6.6\rho^{1/3})$ of the liquid as a function of temperature along the isomorph. The inset demonstrates that the structure becomes more invariant when the correlation coefficient is high.

If the pair potential is an inverse power-law (r^{-n}), the isomorphs are given by $\rho^\gamma/T = $ const. in which $\gamma = n/3$.[8,14] For this reason, γ is referred to as the "density-scaling exponent." In general, γ is state-point dependent.[7,8,63–65] It has been demonstrated that for many systems with pair interaction, including the LJ and the EXP systems, the exponent can be approximated by fitting an *effective* (state-point dependent) inverse power-law to the pair potential as some distance.[66] For the dense phases (liquid and solid), this results in the expression

$$\gamma(\rho, S_{\text{ex}}) \cong -\frac{2}{3} - \frac{r}{3} \frac{v^{(3)}(r)}{v^{(2)}(r)}\bigg|_{r=\Lambda(S_{\text{ex}})\rho^{-1/3}/\sigma}, \quad (16)$$

where $v^{(i)}(r)$ is the ith derivative of the pair potential with respect to r and $\Lambda(S_{\text{ex}})$ is a free parameter for any given isomorph, expected to be close to unity. Under the assumption that Λ is the same for different isomorphs, γ is only a function of density to a good approximation. Figure 6 shows the true γ of Eq. (9) (dots) and the γ estimated from the pair interactions (solid lines) via Eq. (16), using the Λ that yields the correct γ at the reference temperature T_0. The agreement is excellent. Thus, an isomorph can be computed from a single reference state point by integrating Eq. (9) using Eq. (16) with Λ determined at the reference state point by calculating γ from the fluctuations via Eq. (10).
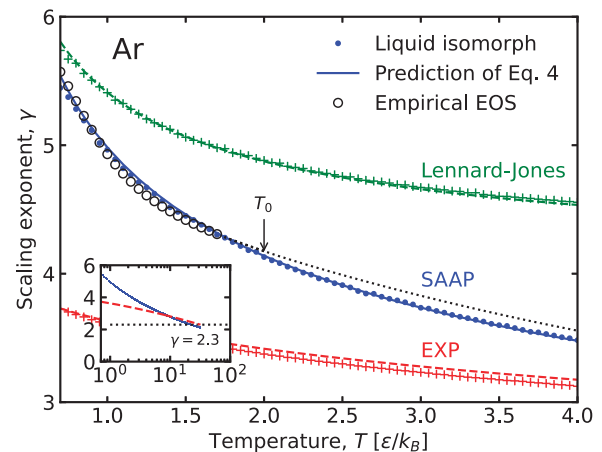

FIG. 6. The blue dots show the density-scaling exponent γ of SAAP with Ar parameters along the liquid isomorph. The blue solid line is the estimate of γ based on using Eq. (16) with $\Lambda(S_{\text{ex}}) = 1.047$. The Λ value is chosen to give the correct γ at the reference temperature $T_0 = 2\varepsilon/k_B$ (indicated with an arrow). The agreement is good for all the investigated state points. The open circles are values from the empirical argon EOS obtained by Tegeler *et al.*[67] The green dashed line is the predictions of Eq. (16) for the LJ potential, and the green + symbols are the exponents computed in simulations at the state points of the liquid isomorph of the LJ potential. The red dashed line and +'s are the same for the EXP potential. The LJ potential gives the best description at low temperatures and the EXP at high temperatures. This is in agreement with the fact that the LJ pair potential gives a good description at low energies, while the EXP potential gives a good description at high temperatures (see Fig. 1). The inset shows γ as a function of T along the liquid isomorph at high temperatures. At temperatures above $T = 21\varepsilon/k_B = 3000$ K, the exponent goes below 2.3. This suggests that the stable crystal phase of argon is bcc at high temperatures, similar to what is observed for the EXP potential.[37]

In this paper, we investigate the fcc solid noting, however, that it is well known that noble elements can form other crystal structures such as hexagonal closed packing (hcp) at higher pressures than investigated here.[68] At very high pressures (high densities and temperatures), the density-scaling exponent γ decreases and approaches that of the EXP potential. As such, the pair potential becomes long ranged compared to the interparticle distance. When $\gamma < 2.3$, it is expected that the body-centered cubic (bcc) crystal becomes thermodynamically stable compared to the closed packed crystals (fcc and hcp).[15,17,69] Hoover and co-workers[15] explained the fcc–bcc–fluid triple point for many metals by the fact that the effective pair potential becomes soft. It was recently shown that the EXP pair potential has a fcc–bcc–fluid triple point[37] located where $\gamma = 2.33(3)$.[70] Since the noble-elements' SAAP is approximated by the EXP potential at high densities, we expect that these elements have an fcc–bcc–fluid triple point where $\gamma \simeq 2.3$. For Ar, we estimate the fcc–bcc–fluid triple point to be at $T = 21\varepsilon/k_B$ = 3000 K (see the inset of Fig. 6). Belonoshko and co-workers argued that this triple point exists for Xe, based on theoretical calculations and re-interpretations of experiments.[71,72] The experiments presented in Ref. 73 were, however, unsuccessful in detecting such a triple point. We note that γ for the LJ potential is 4 in the high-pressure limit, and thus, an fcc–bcc–fluid triple point is not expected to exist.[74] The LJ potential, however, does not describe the noble elements at high pressures since it is too harsh. Moreover, we note that the EXP high-pressure limit of the pair interactions also suggests a re-entrance temperature above which no crystalline phase is stable (see $T^\star$ in Ref. 70).

The density-scaling exponent γ can be determined from thermodynamic data as the ratio between the excess pressure coefficient $\beta_V^{\mathrm{ex}} \equiv (\partial W/\partial T)_V/V$ and the excess isochoric heat capacity per volume $c_V^{\mathrm{ex}} \equiv (\partial U/\partial T)_V/V$,[8]

$$\gamma = \frac{\beta_V^{\mathrm{ex}}}{c_V^{\mathrm{ex}}}. \qquad (17)$$

These two thermodynamic quantities are usually not directly available from experiments. Using standard thermodynamic relations, γ can be rewritten, however, as

$$\gamma = \frac{\gamma_G - k_B/c_V}{1 - 3k_B/2c_V}, \qquad (18)$$

where

$$\gamma_G = \left. \frac{\partial \ln T}{\partial \ln \rho} \right|_S = \frac{\alpha K_T}{c_V} \qquad (19)$$

is the thermodynamic Grüneisen parameter,[38,75–77] c_V is the isochoric heat capacity, α is the thermal expansion coefficient, and K_T is the isothermal bulk modulus. Within the Dulong–Petit approximation, $c_V \simeq 3k_B$, one finds (compare Ref. 78)

$$\gamma \simeq 2\gamma_G - 2/3. \qquad (20)$$

The value of the thermodynamic Grüneisen parameter is $\gamma_G = 2.9$[13,79] near the gas–liquid–solid triple point of Ar. This corresponds to $\gamma = 5.1$, which is in good agreement with the value obtained by the SAAP (Fig. 6). Amoros et al.[79] noticed that γ_G is only a function of density to a good approximation. This is explained by the fact that Λ in Eq. (16) is close to unity for all S_{ex}, making γ

and γ_G functions solely of the density. Thus, γ_G is also only a function of density. This is only expected to be true in dense phases, i.e., for the liquid and the solid. In the gas limit, only temperature is expected to be relevant, as illustrated for the EXP potential in Ref. 16. The reason is that the typical collision distance of gas particles only depends on the temperature. In Fig. 6 (open circles), we compare the γ along the liquid isomorph of the SAAP potential to that of the empirical equation of state (EOS) obtained by Tegeler et al.[67] (this EOS is implemented into the CoolProp software library by Bell et al.[80]). The agreement is good.

To summarize, we have established that (i) the SAAP gives a good representation of Ar, (ii) the SAAP possesses hidden scale invariance near the coexistence line in both the liquid and solid phases, and (iii) the isomorphs can be computed from a reference coexistence point by means of Eq. (16) and Eq. (9).

Next, we apply the isomorph theory of the melting line[25] to SAAP argon.

IV. THEORY OF THE MELTING LINE

Using the LJ system as an example, Ref. 25 showed how the freezing and melting lines, as well as the variation of several properties along these lines, can be calculated from simulations carried out at a single coexistence state point by knowing the solid and liquid isomorphs through this state point. In particular, the coexistence pressure as a function of temperature, $p_m(T)$, can be computed from the liquid and the solid isomorphs through a reference state point on the coexistence line with temperature T_0. This leads[25] to

$$p_m(T) = [C_1(T) + C_2(T) + T\hat{C}_3]/C_4(T), \qquad (21)$$

in which

$$C_1(T) = U_s^I(T) - [T/T_0]U_s^I(T_0) - U_l^I(T) + [T/T_0]U_l^I(T_0),$$

$$C_2(T) = Nk_BT \ln(V_s^{(0)}/V_s^I(T)) - Nk_BT \ln(V_l^{(0)}/V_l^I(T)), \qquad (22)$$

$$\hat{C}_3 = p_0[V_l^{(0)} - V_s^{(0)}]/T_0,$$

and

$$C_4(T) = [V_l^I(T) - V_s^I(T)]. \qquad (23)$$

Here, the superscript "I" indicates values along the isomorphs, the "0" indicates values at the reference state point, the subscript "s" indicates the solid value, and the subscript "l" indicates the liquid value. In Fig. 7(a), we test the prediction of the melting theory for Ar using the liquid and solid isomorphs defined by the reference temperature $T_0 = 2\varepsilon/k_B$ [shown in Fig. 7(b)].

Not only is the pressure variation along the melting line predicted but so are the variations of a number of other properties along the freezing and melting lines—again using only information obtained by simulations at the reference state point. The density of the liquid on the freezing line, ρ_l, is given by

$$\ln \rho_l(T) = \ln \rho_l^I(T) + (W_m(T) - W^I(T))/(\partial W/\partial \ln \rho)_T, \qquad (24)$$

where $W_m = p_m/\rho_l - k_BT$ is the virial at melting. The density of the solid, ρ_s, has an analogous expression. The theoretical prediction is shown in Fig. 7(b) as dots. The prediction is good, though deviations are noted at low temperatures. Similar deviations (but small) are seen also for the LJ system.[25] The deviation from the theory are not unexpected since R [Eq. (15)] is lower near the triple point.
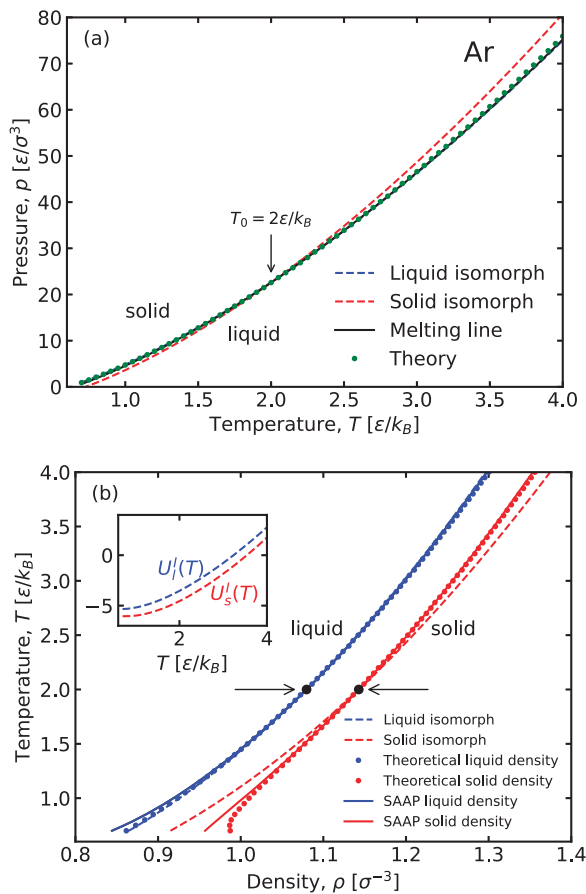
FIG. 7. Applying the melting theory of Ref. 25 to SAAP argon. The prediction is made from the reference state point with temperature $T_0 = 2\varepsilon/k_B$ indicated by arrows. (a) shows the melting line in the pressure-temperature diagram, (b) shows the melting and freezing lines in a temperature-density diagram. The inset of (b) shows the potential energy per particle along the liquid (blue) and solid (red) isomorphs. The statistical errors are small in comparison to the thickness of the lines and symbols for all the shown data.
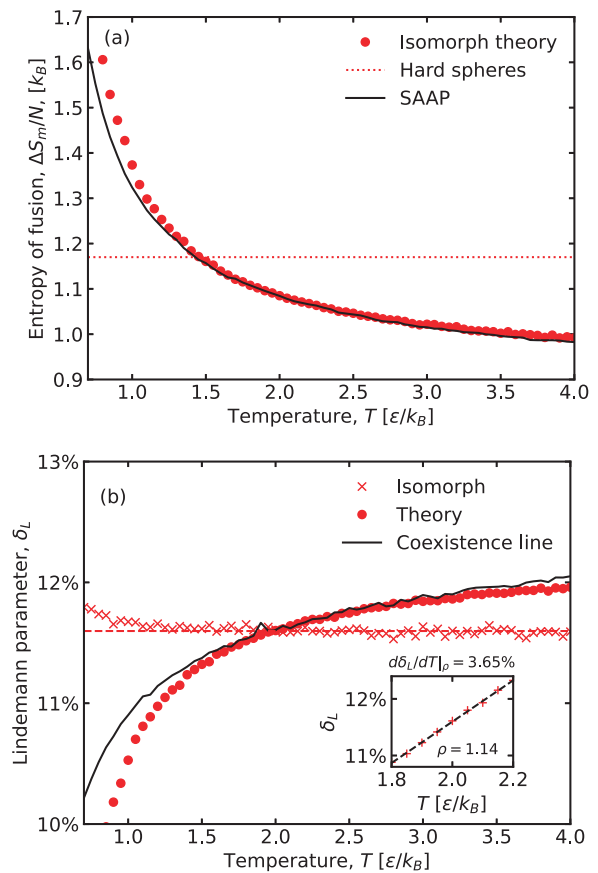

FIG. 8. (a) The entropy of fusion per particle $\Delta S_m/N$ in units of k_B. The solid line is the simulation result for SAAP argon, the dots mark the prediction of the isomorph theory, and the horizontal dotted line is the entropy of fusion of hard-spheres.[81] (b) The Lindemann parameter δ_L of the fcc crystalline solid at melting. The solid line is δ_L along the SAAP coexistence line, and the dots are the theoretical prediction of the isomorph theory. The prediction is made only using information at the reference state point ($T_0 = 2\varepsilon/k_B$). The ×'s are the Lindemann parameter along the isomorph. As expected from the isomorph theory, it is near invariant (red dashed line). The inset shows the simulation data needed for determining $d\delta_L/dT|_\rho = 0.0365$ at the reference temperature, which is used for the isomorph-theory prediction.[25]

Figure 8(a) shows the entropy of fusion ΔS_m per particle along the coexistence line (solid line). The theoretical prediction, shown as red dots, is quite good. For comparison, we note that the hard-sphere picture predicts a constant entropy of fusion. Figure 8(b) shows the Lindemann parameter of the fcc crystal,

$$\delta_L = [\rho/4]^{1/3}\sqrt{\overline{\Delta r^2}/6}, \qquad (25)$$

where

$$\overline{\Delta r^2} = \langle |\mathbf{r}_i(0) - \mathbf{r}_i(t \to \infty)|^2 \rangle \qquad (26)$$

is the root-mean-squared displacement of particles in the crystal at long times[82] ($\langle u^2 \rangle = \overline{\Delta r^2}/3$ in Ref. 82). The +'s in the inset show the Lindemann parameter along the $\rho = 1.14$ isochore. The dashed line is a linear fit that yields $\partial \delta_L/\partial T|_\rho = 0.0365 k_B/\varepsilon$ needed in the theoretical prediction.[25] The theoretical predictions are good for both

ΔS_m and δ_L; however, they both become less accurate at low temperatures. This is related to the relatively poor prediction for the solid density near the triple point [Fig. 7(b)].

V. COEXISTENCE LINES OF NEON, KRYPTON, AND XENON

The solid–liquid coexistence lines of Ne, Kr, and Xe are computed in the same way as for Ar. Figures 9(a)–9(c) show the results. For reference, the light gray lines in each panel show the Ar coexistence line [Fig. 7(a)] and Fig. 9(d) shows results for the LJ model. The dotted red lines are empirical coexistence lines.[68,83] The SAAP potential systematically slightly overestimates the coexistence temperature at a given pressure. This is likely due to missing many-body interactions, as discussed for the case of Ar.
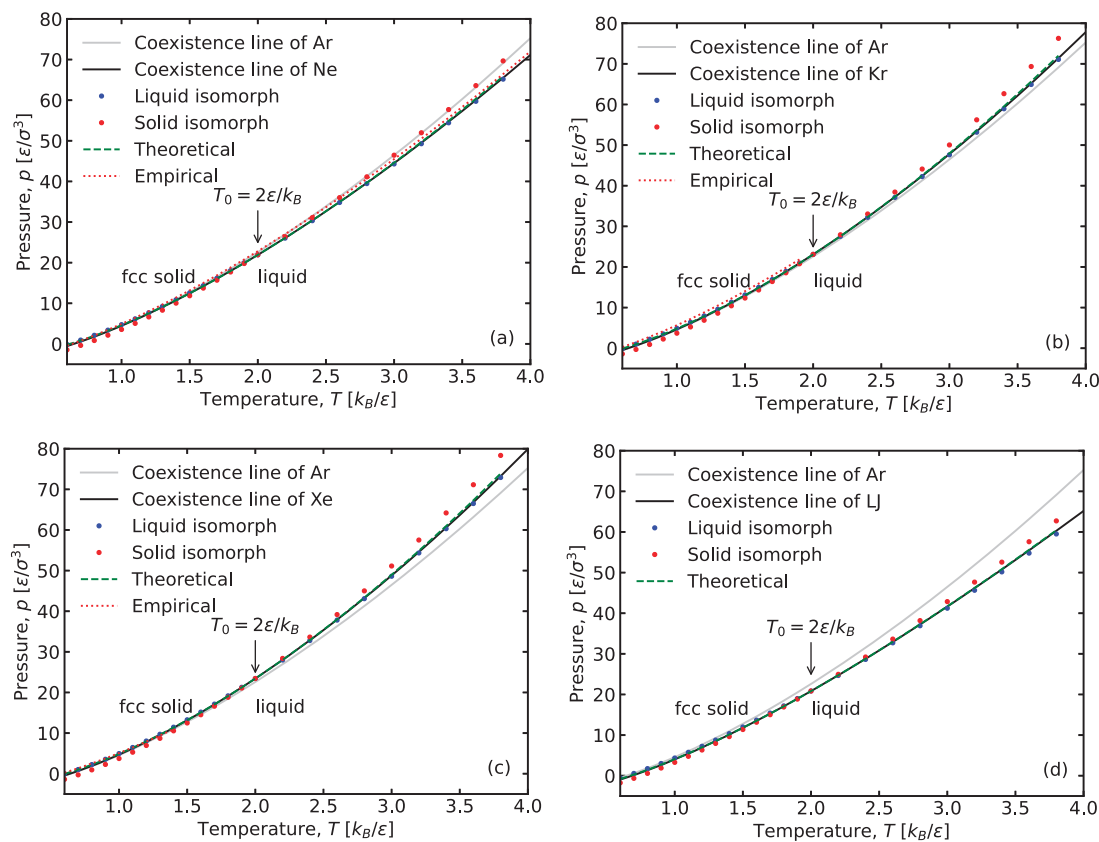
FIG. 9. The solid–liquid coexistence lines in the pressure-temperature plane of (a) neon, (b) krypton, (c) xenon, and (d) the LJ model. For reference, each figure shows the coexistence line of SAAP Ar as gray lines [see Fig. 2(a)]. The dots represent solid and liquid isomorphic state points (generated from the reference state point at $T_0 = 2\varepsilon/k_B$), and the green dashed line is the theoretical prediction of the isomorph theory (see below). Empirical melting lines are shown as red dotted lines.[68,83] The statistical errors are small in comparison to the thickness of the lines and symbols for all the shown data.

Deiters and Sadus investigated the gas–liquid coexistence lines for the SAAP potentials of the noble elements.[52] Here, we compute the coexistence between the liquid and the face-centered cubic (fcc) solid. In all, this information allows one to compute the

gas–liquid–fcc triple points (Table II). The triple-point temperatures of the elements are very similar, ranging from $0.642\,51(35)\varepsilon/k_B$ for Xe to $0.660\,54(5)\varepsilon/k_B$ for Ne. This is not surprising, given the similar shapes of the pair potentials (Fig. 1). However, the SAAP

TABLE II. Thermodynamic data for the SAAP triple points and corresponding empirical values.

		T_{tp} (ε/k)	T_{tp} (K)	ρ_s (σ^{-3})	ρ_s (g/cm³)	ρ_l (σ^{-3})	ρ_l (g/cm³)	ρ_g (σ^{-3})
Ne	SAAP	$0.650\,54(5)$	$27.558(2)$	$0.952\,39(5)$	$1.519\,37(8)$	$0.825\,92(16)$	$1.317\,6(3)$	$0.004\,21(25)$
	empirical	$0.579\,77^a$	24.56	$0.905\,14$	1.444	$0.782\,28$	1.248	
Ar	SAAP	$0.646\,79(34)$	$92.80(5)$	$0.949\,53(5)$	$1.667\,72(9)$	$0.825\,32(35)$	$1.449\,6(6)$	$0.004\,25(25)$
	empirical	$0.584\,04$	83.81	$0.924\,07$	1.623	$0.802\,80$	1.410	
Kr	SAAP	$0.645\,77(54)$	$129.85(9)$	$0.947\,50(2)$	$2.873\,53(6)$	$0.826\,24(26)$	$2.505\,8(8)$	$0.003\,51(28)$
	empirical	$0.575\,73$	115.78	$0.931\,83$	2.826	$0.808\,18$	2.451	
Xe	SAAP	$0.642\,51(35)$	$180.02(10)$	$0.945\,34(4)$	$3.471\,25(15)$	$0.823\,78(15)$	$3.024\,88(55)$	$0.004\,38(11)$
	empirical	$0.575\,94$	161.37	$0.925\,66$	3.399	$0.837\,70$	3.076	
LJ		0.694^b		0.96		0.84		

aEmpirical data are taken from Ref. 85.
bLJ data are taken from Ref. 84.

triple-point temperatures are 10%–12% above the empirical values, and the SAAP triple-point densities of the solids are 2%–5% higher than the empirical values. These systematic deviations are likely due to the missing many-body interactions, as discussed for the case of
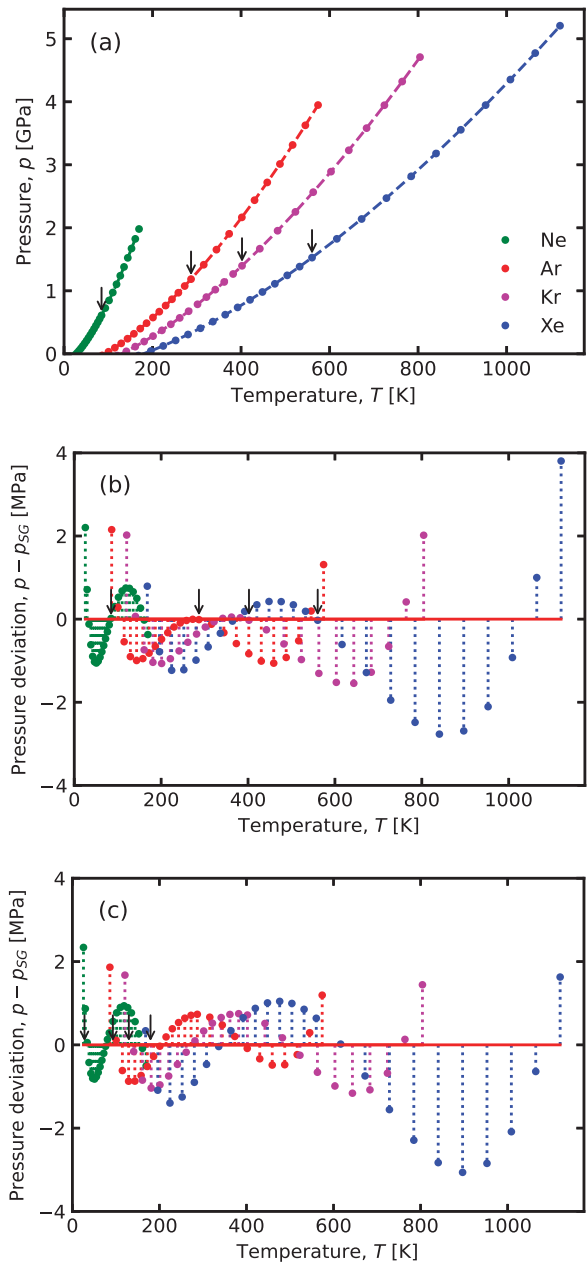

FIG. 10. (a) Fit of the Simon–Glatzel equation [Eq. (27); dashed lines] to the SAAP solid–liquid coexistence line (dots) of Ne (green), Ar (red), Kr (purple), and Xe (blue). The reference state point (T_0, p_0) is indicated with arrows. The parameters in Eq. (27) are given in Table III. (b) Residuals using T_0 as the reference temperature (indicated with arrows). (c) Residuals using p_{ref} = 0 and with the reference temperature T_{ref} as a fitting parameter ($T_{ref} \cong T_{tp}$ is indicated with arrows). The parameters for Eq. (27) are given in Table IV. The statistical errors are small in comparison to the thickness of the line or symbols for all the shown data.

TABLE III. Parameters of the Simon–Glatzel equation [Eq. (27)] of SAAP coexistence state points using $T_{ref} = T_0$ and $p_{ref} = p_0$ as the reference state point. The fit is shown in Fig. 10(a).

	T_0 (K)	p_0 (GPa)	a (GPa)	c
Ne	84.72	0.610 10	0.751	1.4983
Ar	286.98	1.184 98	1.436	1.5473
Kr	402.16	1.396 45	1.681	1.5699
Xe	560.37	1.526 07	1.824	1.5924

argon. The triple-point temperature of the LJ model is above that of the SAAP potential, $0.694\varepsilon/k_B$,[84] which is possibly an effect of the broader range of attraction of the LJ pair potential compared to that of the SAAP (see Fig. 1).

As an aside, we investigate the validity of the Simon–Glatzel equation for the coexistence pressure,[86]

$$p_{SG}(T) = p_{ref} + a\left[\left[T/T_{ref}\right]^c - 1\right]. \tag{27}$$

We first use $T_{ref} = T_0$ and $p_{ref} = p_0$. Figure 10(a) shows fit to the SAAP coexistence lines where the a and c parameters are determined by least-squares fitting (see Table III). The accuracy of the fit is within a few MPa [Fig. 10(b) shows the residuals]. The triple point temperature is often used when fitting empirical data. Table IV gives parameters using $p_{ref} = 0$ and T_{ref} as a third fitting parameter (in addition to a and c). The accuracy of the fit is compatible for the two approaches [Figs. 10(b) and 10(c)]. With the latter procedure, the reference temperature is almost identical to the triple-point temperature: $T_{ref} \cong T_{tp}$ (since the triple point pressure is nearly zero for the relevant pressure scale). Table IV compares the SAAP parameters with parameters from empirical data. The agreement is in general good. The a parameter and T_{ref} of the SAAP fit are systematically lower than the parameters determined from the empirical data. This is likely due to the missing many-body interactions of the SAAP, as discussed for the case of Ar.

TABLE IV. Parameters for the Simon–Glatzel equation [Eq. (27)] of SAAP coexistence state points and empirical data using the triple-point temperature as reference: $T_{ref} = T_{tp}$. For the SAAP results, T_{ref} is treated as a fitting parameter and $p_{ref} = 0$.

		T_{ref} (K)	a (GPa)	c
Ne	SAAP	27.75	0.1409	1.4989
	empirical, Ref. 83	24.55	0.1286	1.4587
Ar	SAAP	92.91	0.2501	1.5487
	empirical, Ref. 68	83.81	0.2245	1.5354
Kr	SAAP	129.64	0.2835	1.5713
	empirical, Ref. 68	115.77	0.2666	1.4951
Xe	SAAP	179.45	0.2966	1.5942
	empirical, Ref. 68	161.40	0.2594	1.4905

VI. HIDDEN SCALE INVARIANCE OF NEON, KRYPTON, AND XENON

Figure 11(a) shows the density-scaling exponents of the elements along the liquid isomorphs plotted as functions of the temperature. At low temperatures, near the triple point, the exponents are 5.6 ± 0.3. This value is close to that of the LJ potential.[7] For SAAP, γ decreases at higher temperatures and densities as for the LJ model; however, the γ variation is larger for the SAAP elements, and γ eventually goes below the LJ infinite-temperature limit of 4. Thus, we conclude that the LJ potential is insufficient in describing the configurational adiabats of the noble elements. The γ's decrease with increasing atomic number. The value of γ can be estimated from the pair potential, and the decrease of γ with increasing atomic number is directly related to the softness of the pair interaction: the softer pair interactions of Xe explain why its γ is lower than that of Ne. Figure 11(b) shows the density-scaling exponents γ of the elements along the solid isomorphs. The conclusions are the same as for the liquids.

Figure 12(a) shows the Pearson correlation coefficients R between the virial W and the potential energy U [Eq. (15)]. The
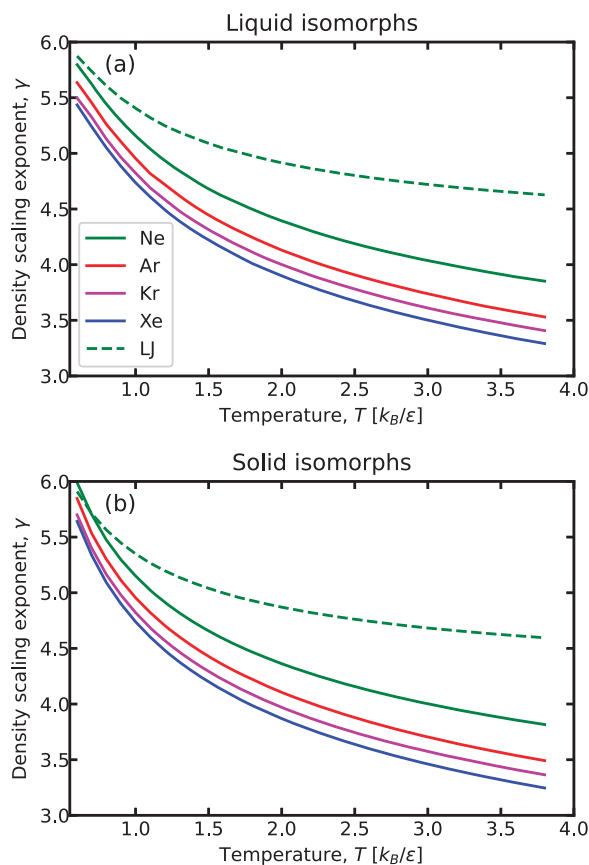

FIG. 11. The density-scaling exponents γ of (a) the liquid isomorphs and (b) the solid isomorphs for the SAAP elements: Ne (green solid line), Ar (red solid line), Kr (violet solid line), Xe (blue solid line), and LJ (green dashed line). The statistical errors are small in comparison to the thickness of the line or symbols for all the shown data.
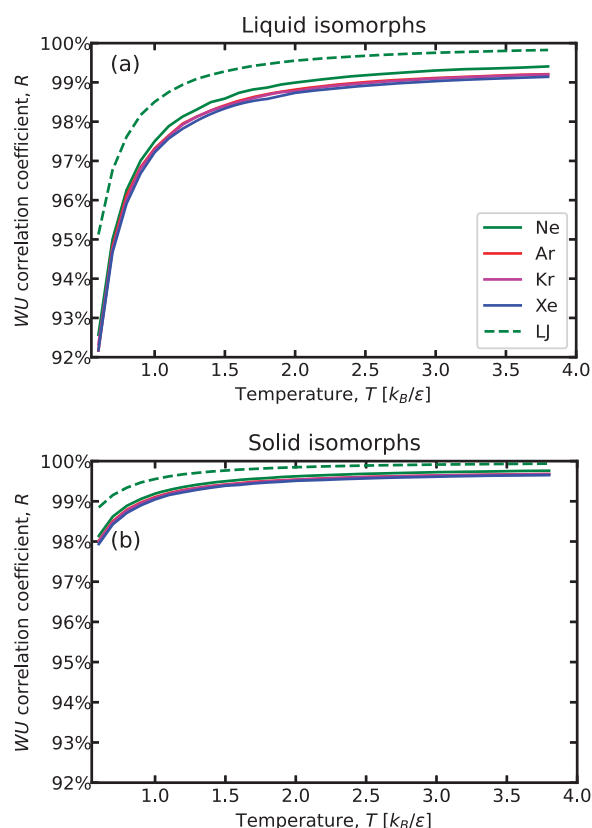

FIG. 12. Pearson correlation coefficient R between the virial W and the potential energy U [Eq. (15)] for the SAAP elements: Ne (green solid line), Ar (red solid line), Kr (violet solid line), Xe (blue solid line), and LJ (green dashed line). R is computed along the liquid (a) and solid (b) isomorphs. The fact that R is close to unity implies that the potential-energy function has hidden scale invariance at the state points in question.[8] The statistical errors are small in comparison to the thickness of the lines for all the shown data.

correlation coefficient is close to unity, $R > 0.92$, demonstrating that the potential-energy function has hidden scale invariance. Thus, the structure, dynamics, and certain thermodynamics quantities are expected to be approximately isomorph invariant (in reduced units). This was demonstrated for Ar above, and we find similar results for the three other elements (results not shown). The WU-correlation coefficient R for SAAP is somewhat smaller than that of the LJ potential [green dashed line in Fig. 12(a)]. Figure 12(b) shows that $R > 0.98$ for the isomorphs of the solid phases.

VII. ISOMORPH THEORY OF THE SOLID–LIQUID COEXISTENCE LINE FOR NEON, KRYPTON, AND XENON

Figures 13(a)–13(c) show the theoretical prediction of the coexistence region's boundaries in the density–temperature plane as green dashed lines. The agreement is quite good, though with some
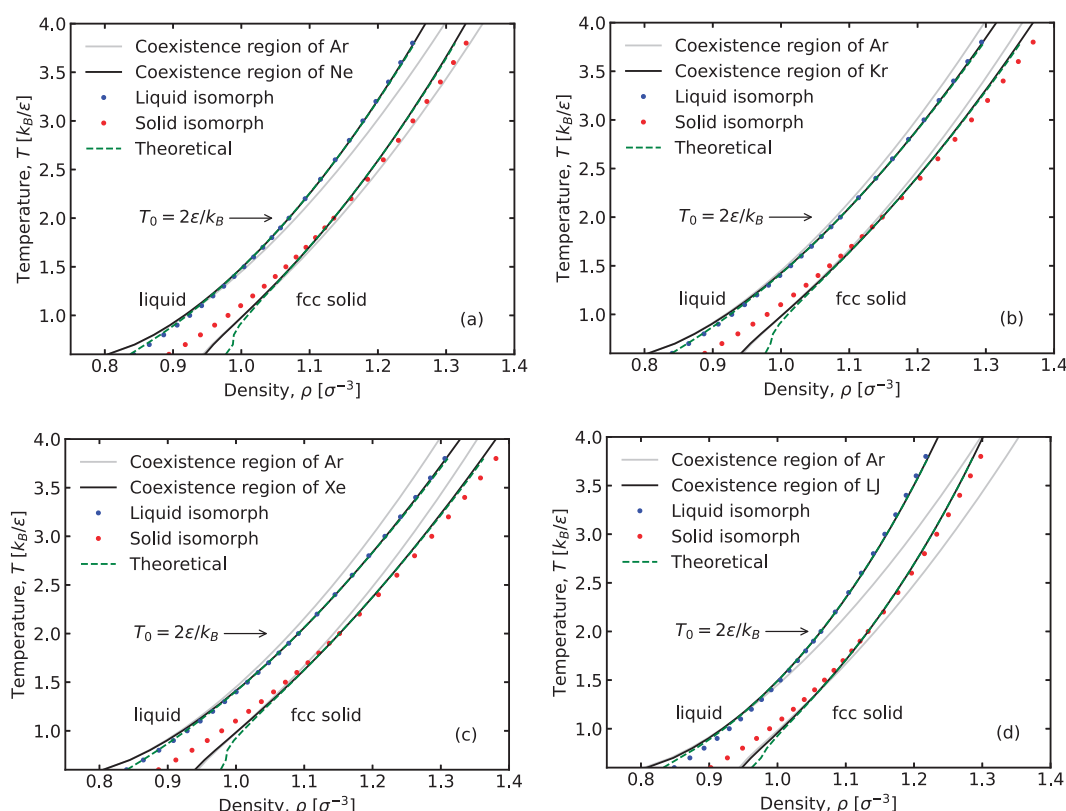
FIG. 13. Full curves show the solid–liquid coexistence region in the density–temperature plane of (a) SAAP neon, (b) SAAP krypton, (c) SAAP xenon, and (d) the LJ model. For comparison, the gray lines delimit the coexistence region of SAAP Ar [see Fig. 2(b)]. The dots are solid and liquid isomorphic state points of the reference temperature $T_0 = 2\varepsilon/k_B$. The green dashed line is the theoretical prediction of the isomorph theory.[25] The prediction is excellent at high densities but less so at low densities near the triple point. The statistical errors are small in comparison to the thickness of the lines and symbols for all the shown data.

deviations at lower temperatures near the triple point temperature. For these temperatures, the density of the solid isomorphs is several percent lower than the density of melting. These deviations may come from the fact that only the first-order terms in the Taylor
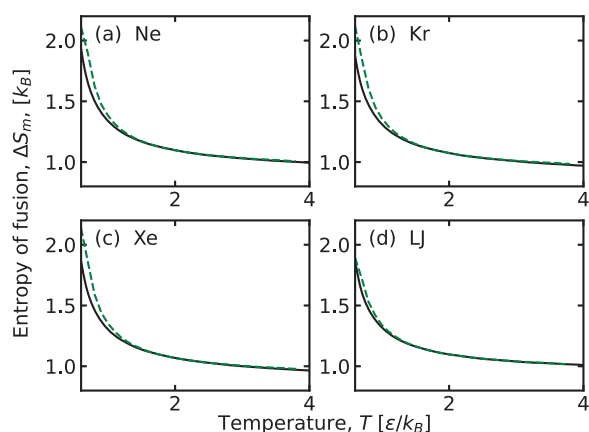

FIG. 14. The entropy of fusion ΔS_m of (a) Ne, (b) Kr, (c) Xe, and (d) LJ. The black solid lines are the ΔS_m's of the SAAP coexistence line, and the green dashed lines are the predictions of the isomorph theory.

expansion were included in the analysis.[25] We leave this for future investigations.

Figures 14(a)–14(c) show the entropy of fusion (ΔS_m) for: Ne, Kr, and Xe, respectively. The accuracy is comparable to that of Ar but slightly worse than that of the LJ model [Fig. 14(d)]. For comparison, we note that hard-sphere based melting models predict ΔS_m to be constant. Thus, the theoretical predictions of the isomorph framework are encouraging.

VIII. CONCLUSION AND OUTLOOK

In summary, we have investigated the solid–liquid coexistence of Ne, Ar, Kr, and Xe using the SAAP. We conclude that the isomorph theory of melting, which has no free parameters except those determined by simulations at the reference temperature, gives accurate predictions for the coexistence line and of variations of properties along this line. An obvious question is how well the isomorph melting theory describes molecular fluids. As a possible starting point, Hellmann provided an analytical potential for the CO_2 molecule based on accurate *ab initio* dimer calculations.[87] Empirical data suggest that the isomorph theory applies to molecular systems,[5,9,55,64,88,89] but the isomorph theory of melting[25] has not yet been tested for such systems.

SUPPLEMENTARY MATERIAL

The supplementary material contains details about the simulation algorithms, raw data, and additional figures.

ACKNOWLEDGMENTS

DATA AVAILABILITY

The data used in this study are available at http://doi.org/10.5281/zenodo.3888373 and in the supplementary material.

REFERENCES

[1] J. P. Hansen and I. McDonald, *Theory of Simple Liquids* (Academic Press, London, 1976).

[2] T. B. Schrøder and J. C. Dyre, "Simplicity of condensed matter at its core: Generic definition of a Roskilde-simple system," J. Chem. Phys. **141**, 204502 (2014).

[3] Y. Rosenfeld, "Relation between the transport coefficients and the internal entropy of simple systems," Phys. Rev. A **15**, 2545–2549 (1977).

[4] C. Alba-Simionesco, A. Cailliaux, A. Alegría, and G. Tarjus, "Scaling out the density dependence of the α relaxation in glass-forming polymers," Europhys. Lett. **68**, 58 (2004).

[5] R. Casalini and C. M. Roland, "Thermodynamical scaling of the glass transition dynamics," Phys. Rev. E **69**, 062501 (2004).

[6] C. M. Roland, S. Hensel-Bielowka, M. Paluch, and R. Casalini, "Supercooled dynamics of glass-forming liquids and polymers under hydrostatic pressure," Rep. Prog. Phys. **68**, 1405–1478 (2005).

[7] U. R. Pedersen, N. P. Bailey, T. B. Schrøder, and J. C. Dyre, "Strong pressure-energy correlations in van der Waals liquids," Phys. Rev. Lett. **100**, 015701 (2008).

[8] N. Gnan, T. B. Schrøder, U. R. Pedersen, N. P. Bailey, and J. C. Dyre, "Pressure-energy correlations in liquids. IV. 'Isomorphs' in liquid phase diagrams," J. Chem. Phys. **131**, 234504 (2009).

[9] D. Gundermann, U. R. Pedersen, T. Hecksher, N. P. Bailey, B. Jakobsen, T. Christensen, N. B. Olsen, T. B. Schrøder, D. Fragiadakis, R. Casalini, C. Michael Roland, J. C. Dyre, and K. Niss, "Predicting the density-scaling exponent of a glass-forming liquid from Prigogine–Defay ratio measurements," Nat. Phys. **7**, 816–821 (2011).

[10] J. C. Dyre, "Hidden scale invariance in condensed matter," J. Phys. Chem. B **118**, 10007–10024 (2014).

[11] A. K. Bacher, T. B. Schrøder, and J. C. Dyre, "Explaining why simple liquids are quasi-universal," Nat. Commun. **5**, 5424 (2014).

[12] J. C. Dyre, "Simple liquids' quasiuniversality and the hard-sphere paradigm," J. Phys.: Condens. Matter **28**, 323001 (2016).

[13] P. Mausbach, A. Köster, and J. Vrabec, "Liquid state isomorphism, Rosenfeld-Tarazona temperature scaling, and Riemannian thermodynamic geometry," Phys. Rev. E **97**, 052149 (2018).

[14] W. G. Hoover, S. G. Gray, and K. W. Johnson, "Thermodynamic properties of the fluid and solid phases for inverse power potentials," J. Chem. Phys. **55**, 1128–1136 (1971).

[15] W. G. Hoover, D. A. Young, and R. Grover, "Statistical mechanics of phase diagrams. I. Inverse power potentials and the close-packed to body-centered cubic transition," J. Chem. Phys. **56**, 2207–2210 (1972).

[16] A. K. Bacher, T. B. Schrøder, and J. C. Dyre, "The EXP pair-potential system. I. Fluid phase isotherms, isochores, and quasiuniversality," J. Chem. Phys. **149**, 114501 (2018).

[17] F. Hummel, G. Kresse, J. C. Dyre, and U. R. Pedersen, "Hidden scale invariance of metals," Phys. Rev. B **92**, 174116 (2015).

[18] D. M. Heyes, D. Dini, L. Costigliola, and J. C. Dyre, "Transport coefficients of the Lennard-Jones fluid close to the freezing line," J. Chem. Phys. **151**, 204502 (2019).

[19] L. Friedeheim, J. C. Dyre, and N. P. Bailey, "Hidden scale invariance at high pressures in gold and five other face-centered-cubic metal crystals," Phys. Rev. E **99**, 022142 (2019).

[20] K. R. Harris, "Thermodynamic or density scaling of the thermal conductivity of liquids," J. Chem. Phys. **153**, 104504 (2020).

[21] I. H. Bell, G. Galliero, S. Delage-Santacreu, and L. Costigliola, "An entropy scaling demarcation of gas- and liquid-like fluid behaviors," J. Chem. Phys. **152**, 191102 (2020).

[22] I. H. Bell, J. C. Dyre, and T. S. Ingebrigtsen, "Excess-entropy scaling in supercooled binary mixtures," Nat. Commun. **11**, 4300 (2020).

[23] H. W. Hansen, F. Lundin, K. Adrjanowicz, B. Frick, A. Matic, and K. Niss, "Density scaling of structure and dynamics of an ionic liquid," Phys. Chem. Chem. Phys. **22**, 14169–14176 (2020).

[24] U. K. Deiters and R. J. Sadus, "Two-body interatomic potentials for He, Ne, Ar, Kr, and Xe from *ab initio* data," J. Chem. Phys. **150**, 134504 (2019).

[25] U. R. Pedersen, L. Costigliola, N. P. Bailey, T. B. Schrøder, and J. C. Dyre, "Thermodynamics of freezing and melting," Nat. Commun. **7**, 12386 (2016).

[26] K. Patkowski and K. Szalewicz, "Argon pair potential at basis set and excitation limits," J. Chem. Phys. **133**, 094304 (2010).

[27] R. J. Bartlett and M. Musiał, "Coupled-cluster theory in quantum chemistry," Rev. Mod. Phys. **79**, 291–352 (2007).

[28] A. E. Nasrabad, R. Laghaei, and U. K. Deiters, "Prediction of the thermophysical properties of pure neon, pure argon, and the binary mixtures neon-argon and argon-krypton by Monte Carlo simulation using *ab initio* potentials," J. Chem. Phys. **121**, 6423–6434 (2004).

[29] P. Cársky, J. Paldus, and J. Pittner, *Recent Progress in Coupled Cluster Methods: Theory and Applications*, Challenges and Advances in Computational Chemistry and Physics (Springer Netherlands, 2010).

[30] J. L. Cacheiro, B. Fernández, D. Marchesan, S. Coriani, C. Hättig, and A. Rizzo, "Coupled cluster calculations of the ground state potential and interaction induced electric properties of the mixed dimers of helium, neon and argon," Mol. Phys. **102**, 101–110 (2004).

[31] E. Pahl, F. Calvo, L. Koči, and P. Schwerdtfeger, "Accurate melting temperatures for neon and argon from *ab initio* Monte Carlo simulations," Angew. Kemi **47**, 8207–8210 (2008).

[32] B. Jäger, R. Hellmann, E. Bich, and E. Vogel, "State-of-the-art *ab initio* potential energy curve for the krypton atom pair and thermophysical properties of dilute krypton gas," J. Chem. Phys. **144**, 114304 (2016).

[33] O. R. Smits, P. Jerabek, E. Pahl, and P. Schwerdtfeger, "First-principles melting of krypton and xenon based on many-body relativistic coupled-cluster interaction potentials," Phys. Rev. B **101**, 104103 (2020).

[34] A. Ahmed and R. J. Sadus, "Effect of potential truncations and shifts on the solid-liquid phase coexistence of Lennard-Jones fluids," J. Chem. Phys. **133**, 124515 (2010).

[35] M. van Thiel and B. J. Alder, "Shock compression of argon," J. Chem. Phys. **44**, 1056–1065 (1966).

[36] A. K. Bacher, T. B. Schrøder, and J. C. Dyre, "The EXP pair-potential system. II. Fluid phase isomorphs," J. Chem. Phys. **149**, 114502 (2018).

[37] U. R. Pedersen, A. K. Bacher, T. B. Schrøder, and J. C. Dyre, "The EXP pair-potential system. III. Thermodynamic phase diagram," J. Chem. Phys. **150**, 174501 (2019).

[38] K. Nagayama, *Introduction to the Grüneisen Equation of State and Shock Thermodynamics* (Amazon, 2011).

[39] N. P. Bailey, T. S. Ingebrigtsen, J. S. Hansen, A. A. Veldhorst, L. Bøhling, C. A. Lemarchand, A. E. Olsen, A. K. Bacher, L. Costigliola, U. R. Pedersen, H. Larsen, J. C. Dyre, and T. B. Schrøder, "RUMD: A general purpose molecular dynamics package optimized to utilize GPU hardware down to a few thousand particles," SciPost Phys. **3**, 038 (2017), the webpage for the RUMD software package is http://rumd.org.

[40] F. Datchi, P. Loubeyre, and R. LeToullec, "Extended and accurate determination of the melting curves of argon, helium, ice (H_2O), and hydrogen (H_2)," Phys. Rev. B **61**, 6535–6546 (2000).

[41] U. R. Pedersen, F. Hummel, G. Kresse, G. Kahl, and C. Dellago, "Computing Gibbs free energy differences by interface pinning," Phys. Rev. B **88**, 094101 (2013).

[42] U. R. Pedersen, "Direct calculation of the solid-liquid Gibbs free energy difference in a single equilibrium simulation," J. Chem. Phys. **139**, 104102 (2013).

[43] V. Thapar and F. A. Escobedo, "Extensions of the interfacial pinning method and application to hard core systems," J. Chem. Phys. **141**, 124117 (2014).

[44] U. R. Pedersen, F. Hummel, and C. Dellago, "Computing the crystal growth rate by the interface pinning method," J. Chem. Phys. **142**, 044104 (2015).

[45] B. Cheng, E. A. Engel, J. Behler, C. Dellago, and M. Ceriotti, "*Ab initio* thermodynamics of liquid and solid water," Proc. Natl. Acad. Sci. U. S. A. **116**, 1110–1115 (2019).

[46] R. S. Newman, S. Nola, J. Dshemuchadse, and S. C. Glotzer, "Shape-controlled crystallisation pathways in dense fluids of CCP-forming hard polyhedra," Mol. Phys. **117**, 3819–3826 (2019).

[47] K. G. Steenbergen, E. Pahl, and P. Schwerdtfeger, "Accurate, large-scale density functional melting of Hg: Relativistic effects decrease melting temperature by 160 K," J. Phys. Chem. Lett. **8**, 1407–1412 (2017).

[48] Y. Zou, S. Xiang, and C. Dai, "Investigation on the efficiency and accuracy of methods for calculating melting temperature by molecular dynamics simulation," Comput. Mater. Sci. **171**, 109156 (2020).

[49] L.-F. Zhu, J. Janssen, S. Ishibashi, F. Körmann, B. Grabowski, and J. Neugebauer, "A fully automated approach to calculate the melting temperature of elemental crystals," Comput. Mater. Sci. **187**, 110065 (2021).

[50] W. H. Press, S. A. Teukolsky, W. T. Vetterling, and B. P. Flannery, *Numerical Recipes*, The Art of Scientific Computing, 3rd ed. (Cambridge University Press, USA, 2007).

[51] D. A. Kofke, "Direct evaluation of phase coexistence by molecular simulation via integration along the saturation line," J. Chem. Phys. **98**, 4149–4162 (1993).

[52] U. K. Deiters and R. J. Sadus, "Fully a priori prediction of the vapor-liquid equilibria of Ar, Kr, and Xe from *ab initio* two-body plus three-body interatomic potentials," J. Chem. Phys. **151**, 034509 (2019).

[53] B. M. Axilrod and E. Teller, "Interaction of the van der Waals type between three atoms," J. Chem. Phys. **11**, 299–300 (1943).

[54] L. Wang and R. J. Sadus, "Relationships between three-body and two-body interactions in fluids and solids," J. Chem. Phys. **125**, 144509 (2006).

[55] Y. Hiwatari, H. Matsuda, T. Ogawa, N. Ogita, and A. Ueda, "Molecular dynamics studies on the soft-core model," Prog. Theor. Phys. **52**, 1105–1123 (1974).

[56] J. C. Dyre, "Perspective: Excess-entropy scaling," J. Chem. Phys. **149**, 210901 (2018).

[57] I. H. Bell, "Probing the link between residual entropy and viscosity of molecular fluids and model potentials," Proc. Natl. Acad. Sci. U. S. A. **116**, 4070–4079 (2019).

[58] E. Detmar, S. Yazdi Nezhad, and U. K. Deiters, "Determination of the residual entropy of simple mixtures by Monte Carlo simulation," Langmuir **33**, 11603–11610 (2017).

[59] I. Prigogine and R. R. Defay, *Chemical Thermodynamics* (Longman, 1954).

[60] J. Prausnitz, R. Lichtenthaler, and E. G. de Azevedo, *Molecular Thermodynamics of Fluid-Phase Equilibria* (Pearson, 1999).

[61] W. P. Krekelberg, J. Mittal, V. Ganesan, and T. M. Truskett, "How short-range attractions impact the structural order, self-diffusivity, and viscosity of a fluid," J. Chem. Phys. **127**, 044502 (2007).

[62] S. N. Chakraborty and C. Chakravarty, "Entropy, local order, and the freezing transition in Morse liquids," Phys. Rev. E **76**, 011201 (2007).

[63] A. Sanz, T. Hecksher, H. W. Hansen, J. C. Dyre, K. Niss, and U. R. Pedersen, "Experimental evidence for a state-point-dependent density-scaling exponent of liquid dynamics," Phys. Rev. Lett. **122**, 055501 (2019).

[64] D. Fragiadakis and C. M. Roland, "Intermolecular distance and density scaling of dynamics in molecular liquids," J. Chem. Phys. **150**, 204501 (2019).

[65] R. Casalini and T. C. Ransom, "On the pressure dependence of the thermodynamical scaling exponent γ," Soft Matter **16**, 4625–4631 (2020).

[66] L. Bøhling, N. P. Bailey, T. B. Schrøder, and J. C. Dyre, "Estimating the density-scaling exponent of a monatomic liquid from its pair potential," J. Chem. Phys. **140**, 124510 (2014).

[67] C. Tegeler, R. Span, and W. Wagner, "A new equation of state for argon covering the fluid region for temperatures from the melting line to 700 K at pressures up to 1000 MPa," J. Phys. Chem. Ref. Data **28**, 779–850 (1999).

[68] A. G. M. Ferreira and L. Q. Lobo, "The fusion curves of xenon, krypton, and argon," J. Chem. Thermodyn. **40**, 618–624 (2008).

[69] S. A. Khrapak and G. E. Morfill, "Fcc-bcc-fluid triple point for model pair interactions with variable softness," Europhys. Lett. **100**, 66004 (2012).

[70] A. K. Bacher, U. R. Pedersen, T. B. Schrøder, and J. C. Dyre, "The EXP pair-potential system. IV. Isotherms, isochores, and isomorphs in the two crystalline phases," J. Chem. Phys. **152**, 094505 (2020).

[71] A. B. Belonoshko, R. Ahuja, and B. Johansson, "Molecular dynamics study of melting and fcc-bcc transitions in Xe," Phys. Rev. Lett. **87**, 165505 (2001).

[72] A. B. Belonoshko, "Triple fcc-bcc-liquid point on the Xe phase diagram determined by the *n*-phase method," Phys. Rev. B **78**, 174109 (2008).

[73] M. Ross, R. Boehler, and P. Söderlind, "Xenon melting curve to 80 Gpa and $5p–d$ hybridization," Phys. Rev. Lett. **95**, 257801 (2005).

[74] V. N. Bondarev and D. V. Tarasevych, "Thermodynamic stability boundaries of 'classical' noble-gas crystals and the polymorphism problem," Low Temp. Phys. **37**, 595–603 (2011).

[75] E. Grüneisen, "Theorie des festen Zustandes einatomiger Elemente," Ann. Phys. **344**, 257–306 (1912).

[76] P. Mausbach and H.-O. May, "Direct molecular simulation of the Grüneisen parameter and density scaling exponent in fluid systems," Fluid Phase Equilib. **366**, 108–116 (2014).

[77] P. Mausbach, A. Köster, G. Rutkai, M. Thol, and J. Vrabec, "Comparative study of the Grüneisen parameter for 28 pure fluids," J. Chem. Phys. **144**, 244505 (2016).

[78] R. Casalini, U. Mohanty, and C. M. Roland, "Thermodynamic interpretation of the scaling of the dynamics of supercooled liquids," J. Chem. Phys. **125**, 014505 (2006).

[79] J. Amoros, J. R. Solana, and E. Villar, "Temperature, pressure and volume dependence of the Grüneisen parameter of dense gaseous and liquid argon," Mater. Chem. Phys. **20**, 255–260 (1988).

[80] I. H. Bell, J. Wronski, S. Quoilin, and V. Lemort, "Pure and pseudo-pure fluid thermophysical property evaluation and the open-source thermophysical property library CoolProp," Ind. Eng. Chem. Res. **53**, 2498–2508 (2014).

[81] B. J. Alder, W. G. Hoover, and D. A. Young, "Studies in molecular dynamics. V. High-density equation of state and entropy for hard disks and spheres," J. Chem. Phys. **49**, 3688–3696 (1986).

[82] S.-N. Luo, A. Strachan, and D. C. Swift, "Vibrational density of states and Lindemann melting law," J. Chem. Phys. **122**, 194709 (2005).

[83] W. L. Vos, J. A. Schouten, D. A. Young, and M. Ross, "The melting curve of neon at high pressure," J. Chem. Phys. **94**, 3835–3838 (1991).

[84] E. A. Mastny and J. J. de Pablo, "Melting line of the Lennard-Jones system, infinite size, and full potential," J. Chem. Phys. **127**, 104504 (2007).

[85] G. L. Pollack, "The solid state of rare gases," Rev. Mod. Phys. **36**, 748–791 (1964).

[86] F. Simon and G. Glatzel, "Bemerkungen zur Schmelzdruckkurve," Z. Anorg. Allg. Chem. **178**, 309–312 (1929).

[87] R. Hellmann, "*Ab initio* potential energy surface for the carbon dioxide molecule pair and thermophysical properties of dilute carbon dioxide gas," Chem. Phys. Lett. **613**, 133–138 (2014).

[88] H. W. Hansen, A. Sanz, K. Adrjanowicz, B. Frick, and K. Niss, "Evidence of a one-dimensional thermodynamic phase diagram for simple glass-formers," Nat. Commun. **9**, 518 (2018).

[89] Z. Wojnarowska, M. Musiał, S. Cheng, J. Gapinski, A. Patkowski, J. Pionteck, and M. Paluch, "Revealing fast proton transport in condensed matter by means of density scaling concept," J. Phys. Chem. C **124**, 15749–15756 (2020).